PCCP

ROYAL SOCIETY OF CHEMISTRY

PAPER

View Article Online
View Journal | View Issue

Cite this: *Phys. Chem. Chem. Phys.*, 2022, **24**, 12208

Light modulation based on the enhanced Kerr effect in molybdenum disulfide nanostructures with curved features†

Tianlun Li,[a] Xiaodie Li,[a] Duorui Gao,[bc] Jianyong Mao,[a] Yaping Hou,[a] Hui Chen,[a] Feng Li,[a] Yanpeng Zhang,[a] Jixiang Fang[a] and Lei Zhang *[a]

Received 23rd January 2022,
Accepted 30th April 2022

DOI: 10.1039/d2cp00374k

rsc.li/pccp

A novel type of molybdenum disulfide (MoS_2) nanoparticles (NPs) was chemically synthesized, which possessed curved features with three-dimensional (3D) freedom compared with planar two-dimensional (2D) materials. Due to the introduction of curved features, the synthesized NPs exhibited a strongly enhanced nonlinear refractive index ($n_2 \sim 10^{-5}$ cm^{-2} W^{-1}) and third-order susceptibility ($\chi^{(3)} \sim 10^{-7}$ esu), which were experimentally verified by the spatial self-phase modulation effect in the visible wavelength range. Both the nonlinear parameters were two orders of magnitude higher than their planar MoS_2 nanostructure counterparts. In addition, the relative change of the effective nonlinear refractive index $\Delta n_2/n_2$ was found to be distinctly dependent on the intensity of the applied electromagnetic field. Moreover, an all-optical modulation was experimentally realized based on the spatial cross-phase modulation effect. Our results demonstrate planar MoS_2 materials with 3D features as potential candidates for next generation all-optical applications and open a substantial approach for the design of efficient nanomaterials with favorable optical nonlinearity.

Introduction

Nonlinear optics (NLO), focusing on the interaction between light and nonlinear media, is of great benefit to various photonic technologies, such as frequency conversion, ultrafast pulse generation and all-optical signal control.[1–4] Investigating the nonlinear optical process in two-dimensional (2D) materials evokes ever-increasing scientific potential towards diverse on-chip optoelectronic applications, which are so far challenging to realize by utilizing conventional bulk media. Continuously finding and exploring novel 2D materials with excellent optical nonlinearity has pronounced significance in providing exciting prospects to new photonic applications.

As the most popular member of 2D layered materials beyond graphene, transition metal dichalcogenides (TMDs) show attractive tunable and controllable optical and electrical characteristics due to their layer-dependent bandgap and multiple exciton-involved light–matter interaction mechanisms, which open a new pathway for fabricating novel optoelectronic devices, such as light-emitting devices, detectors and modulators.[5–8] Few-layer TMDs, formed by several monolayer 2D materials *via* van der Waals forces, tackle the upcoming requirements of future chip-integrated nanophotonic devices by avoiding the lattice mismatch problem brought about by conventional materials.[9]

So far, the optical nonlinearity of TMDs is mainly studied based on diverse planar 2D nanostructures, such as nanosheets or nanoflakes.[10,11] In fact, in addition to the planar shapes, number of layers, and material quality of TMDs, their geometric characteristics also greatly affect their NLO properties.[12,13] Due to the increase of localized optical fields or the decrease of effective mass caused by the change of geometric morphology, light–matter interaction has been significantly enhanced.[13] Curved geometric features of inorganic nanoparticles (NPs) introduce additional freedom to control and enhance the light–matter interaction strength.[14]

The third-order NLO response has been widely discussed using third-order harmonic generation (THG) and Z-scan techniques. In contrast, spatial self-phase modulation (SSPM) is another effective and more straightforward approach to explore third-order NLO effects. By investigating the evolution of multiple diffraction patterns and their distortions under different experimental conditions, the third-order nonlinear properties

[a] *Key Laboratory of Physical Electronics and Devices of Ministry of Education & Shaanxi Key Laboratory of Information Photonic Technique, School of Electronic Science and Engineering, Xi'an Jiaotong University, Xi'an 710049, China. E-mail: eiezhanglei@xjtu.edu.cn*

[b] *State Key Laboratory of Transient Optics and Photonics, Xi'an Institute of Optics and Precision Mechanics of CAS, Xi'an 710119, China*

[c] *University of Chinese Academy of Sciences, Beijing 100049, China*

† Electronic supplementary information (ESI) available. See DOI: https://doi.org/10.1039/d2cp00374k

have been clearly unveiled in various 2D materials.[15] Furthermore, optical switching/modulation devices based on 2D materials are also designed using another third-order nonlinearity, *i.e.*, spatial cross-phase modulation (SXPM). SXPM occurs when the probe light suffers additional phase variation caused by another co-propagating pump light, which also suggests that the nonlinear optical phase change arises due to the interaction between two spatial beams in nonlinear materials.[16]

Herein, the third-order nonlinear optical properties of molybdenum disulfide (MoS_2) NPs, synthesized using hard mesoporous silica, are experimentally investigated using the SSPM effect at the visible range. The deformation of SSPM patterns from the MoS_2 NP dispersion has also been recorded and analyzed, which is proportionally associated with the effective nonlinear refractive index of the dispersion. Significantly, the nonlinear refractive index n_2 and third-order susceptibility $\chi^{(3)}$ of MoS_2 NPs show orders of magnitude higher nonlinear responses compared with their counterpart planar 2D materials. Besides, an all-optical modulation has also been demonstrated based on the SXPM effect. Our results verify an enhancement of the NLO response by appending curved features to planar 2D materials. Such a mechanism offers a substantial foundation for improving NLO performance with nanoscale materials and applying them in new optical control devices.

Experiments

Preparation and characterization of the MoS_2 NPs

The MoS_2 NPs were chemically synthesized using ordered three-dimensional (3D) mesoporous silica (EP-FDU-12) as hard templates.[14] The precursor, *i.e.*, phosphomolybdic acid (PMA), is incorporated into the template *via* a solvent evaporation process. In a typical procedure, 10 mg of the EP-FDU-12 silica template are immersed and dispersed into an ethanol solution of PMA (20 mM, 1 mL) under stirring for 10 min. The mixture is dried at 40 °C until the ethanol is fully evaporated. After complete drying, the obtained fluorescent-yellow powder of the PMA/EP-FDU-12 silica template composites is put into a tube furnace for reductive sulfuration. The furnace is heated to 650 °C at a rate of 5 °C min^{-1} under a 5% H_2S/95% N_2 atmosphere and maintained at this temperature for 1 h. The tube furnace is connected to a collector with sodium hydroxide solution to react with excess H_2S gas. After cooling down the furnace to room temperature, the dark brown MoS_2/EP-FDU-12 powder is collected and treated with 5 mL 4 wt% HF aqueous solution to etch the silica. Finally, the MoS_2 NPs are collected by washing with water and ethanol. The average diameter of the pores and thickness of the wall are 27 and 5 nm, respectively.

As shown in Fig. 1(a and b), the transmission electron microscopy (TEM, JEOL, JSM-2100F) images of the synthesized MoS_2 NPs reveal a 3D featured morphology with an average diameter of ~27 nm and curved multilayered features with a layer number larger than 5, which excludes the quantum size effect.[17] The TEM images also depict that the MoS_2 NPs display

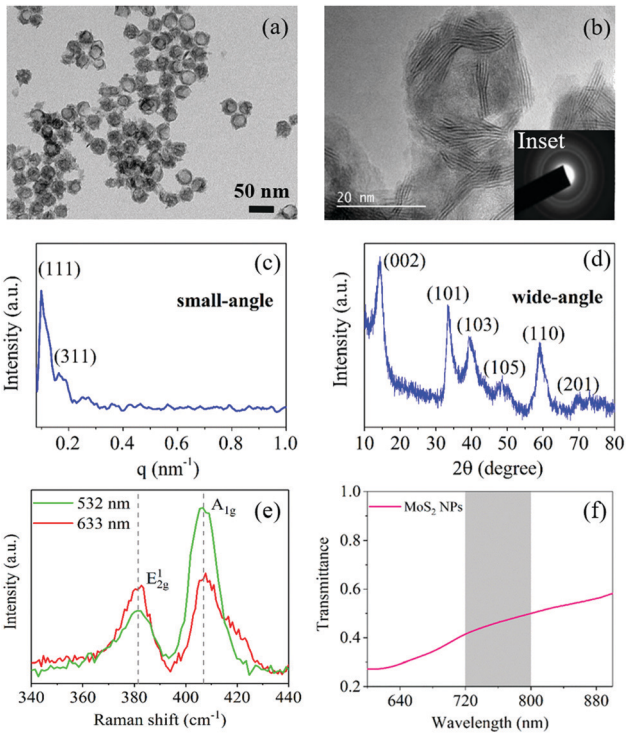

Fig. 1 Structure of the synthesized MoS_2 NPs and their characterization. (a) Low-magnification transmission electron microscopy image and (b) high-resolution transmission electron microscopy image. Inset: Selected area electron diffraction image of the synthesized MoS_2 NPs. (c) Small-angle and (d) wide angle X-ray diffraction patterns of the synthesized MoS_2 NPs. (e) Raman spectra of the MoS_2 NP dispersions excited by 633 and 532 nm lasers. (f) Transmittance of the MoS_2 NP dispersions. The interesting wavelength range is highlighted by the grey area.

a monodispersed spherical structure with good uniformity. The selected area electron diffraction (SAED) pattern shows the polycrystalline feature of the MoS_2 NPs. The small-angle (SAXS, Anton Paar SAXSpoint 2.0) and wide-angle (Bruker, d8 advance) X-ray diffraction (XRD) patterns are shown in Fig. 1(c and d). The small-angle diffraction patterns displayed typically coincide with the SAXS pattern of the reported EP-FDU-12 silica template, and belong to the face-centered-cubic structure. According to the diffraction peaks of the (111) and (311) planes, the interplanar spacings are d_{111} = 25.12 nm and d_{311} = 13.08 nm, corresponding to the cell parameters of 43.50 nm and 43.38 nm, respectively. The diffraction peaks in the X-ray diffraction (XRD) pattern (Fig. 1(d)) are indexed by (002), (101), (103), (105), (110) and (201), corresponding to the standard MoS_2 crystal (JCPDS card No: 37-1492). No other diffraction peaks belonging to PMA, Mo, MoO_3 or MoO_2 are observed, indicating the complete transformation of PMA to MoS_2.[18,19] Two Raman peaks are located at ~382 and ~407 cm^{-1} under the excitations of 532 and 633 nm continuous-wave (CW) lasers, as shown in Fig. 1(e). These two modes correspond to the E^1_{2g} and A_{1g} vibration modes, which can be attributed to the in-plane vibration mode and the out-of-plane vibrations of Mo and S, respectively.[20] Fig. 1(f) shows the transmittance spectrum of the MoS_2 NP dispersions ranging from 600–900 nm (Andor

SR500I), which was used to characterize the effective number of MoS_2 layers in the SSPM experiment.

Results and discussion

n_2 and $\chi^{(3)}$ for the 3D featured MoS_2 NPs

As shown in Fig. 2(a), a femtosecond (fs) pulsed laser with a tuning range of 680–1080 nm (Coherent, Chameleon Ultra II, repetition frequency 80 MHz, pulse width 100 fs at 800 nm) was focused onto the MoS_2 NP suspension by a lens with a focal length of 150 mm. The $1/e^2$ intensity diameter of the laser beam was 800 μm at the front surface of the quartz cuvette that held the MoS_2 NP suspension. The incident power could be controlled by a set of neutral density (ND) filters. When the focused laser illuminated the quartz cuvette of the sample, the self-focusing effect induced by the strong nonlinearity of the MoS_2 NP dispersions made the beam converge rapidly to reach a minimum diameter after propagating several millimeters inside the cuvette, which had a negligible influence on the SSPM experiment.[15] Then, the beam continued to propagate with a slight increase in the beam diameter, as its intensity decreased due to the absorption and light scattering. After exiting the cuvette, the laser beam diverged into a set of coaxial cones, which were recorded by a charge coupled device (CCD) camera as concentric rings, as shown in Fig. 2(b). Both the intensity and width of the ring stripes increased as the ring diameter got larger, which was independent of the wavelength. Interestingly, the diffraction patterns initially spread to perfect concentric rings right after the laser beam traversed the cuvette. Afterwards, these rings instantly grew vertically and horizontally to a maximum geometric size within approximately 0.8 seconds with an incident laser intensity of 9 W cm^{-2}. Subsequently, the diffraction rings rapidly collapsed vertically towards their center, and finally became stable after about 3.55 seconds. Fig. 2(c) shows the typical transformation timeline of the diffraction pattern with a wavelength of 800 nm. The vertical diameter almost distorted to half of the maximum one, while the horizontal diameter was basically unchanged. The third-order nonlinearity was investigated when the number of rings became stable. To eliminate the influence of the nonlinear response from the solvent, the same experiment was carried out by replacing the solution with pure ethanol and deionized water, and no diffraction pattern was observed.

The SSPM phenomenon is essentially caused by the optical Kerr effect,[15] which is recognized as a spatial analogue of the spectral broadening effect due to the self-phase modulation arising from the laser-induced refractive index change.[21] The refractive index of the MoS_2 NP dispersions can be defined as $n = n_0 + n_2 I$, where $n_0 = 1.3$ is the linear refractive index of the liquid environment, *i.e.*, ethanol, n_2 is the nonlinear refractive index, and I stands for the electric field intensity.

From a microscopic perspective, each MoS_2 NP is polarized under the excitation of the applied field, so that they are aligned along the direction of the field. The uniform polarization of the NPs leads to the interference phenomenon, and finally forms the SSPM rings. With the enhancement of the applied optical field, the number of polarized NPs continues to increase. However, since the total number of NPs is constant inside the sample, the SSPM effect will finally saturate when the NPs are all activated by external optical field.

Fig. 3(a) shows the intensity dependence of the ring number N for different wavelengths. It is obvious that N increases approximately linearly with the applied optical field intensity I, as the fitting slope $S = dN/dI$ of the data before saturation

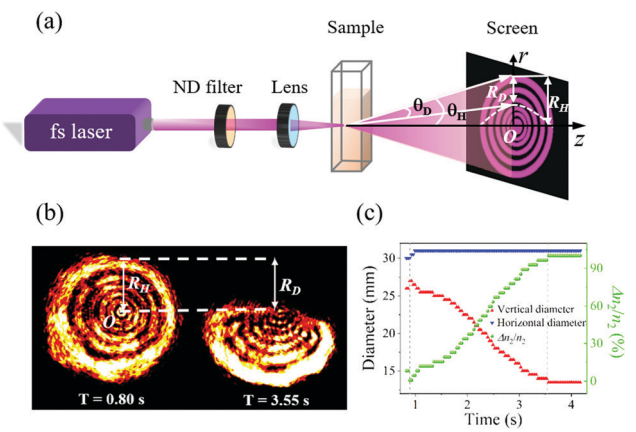

Fig. 2 (a) Schematic of the experimental setup for SSPM. (b) Images of the distortion for the diffraction ring patterns excited by a fs-pulse laser at λ = 800 nm. (c) Evolution of the diameter of the outermost SSPM ring along the vertical and horizontal directions and $\Delta n_2/n_2$ at λ = 800 nm.

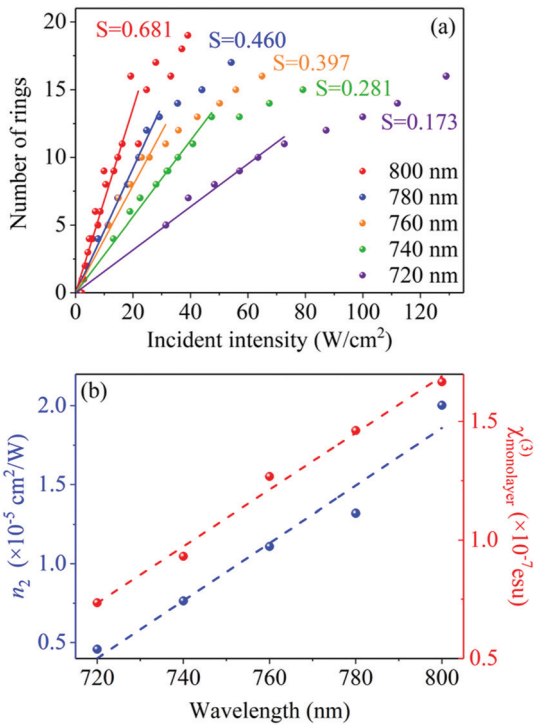

Fig. 3 (a) Dependence of the number of SSPM rings N on the laser intensity I at different wavelengths. (b) Dependence of the nonlinear refractive index and third-order susceptibility of monolayer MoS_2 NPs on the wavelength.

varies with the incident wavelength. The values of n_2 can be obtained as following

$$n_2 = \frac{\lambda}{2n_0 L_{\text{eff}}} \cdot \frac{\mathrm{d}N}{\mathrm{d}I} \quad (1)$$

which is estimated as 1×10^{-5} cm^{-2} W^{-1}, two orders of magnitude higher than the counterpart flat MoS_2 nanosheets.[10] The third-order susceptibility $\chi^{(3)}_{\text{total}}$ can be defined as

$$\chi^{(3)}_{\text{total}} = \frac{\lambda c n_0 S}{2.4 \times 10^4 \times \pi^2 L_{\text{eff}}} \quad (2)$$

Since $E_{\text{total}} = \sum_{i=1}^{N_{\text{eff}}} E_i \approx N_{\text{eff}} E_{\text{monolayer}}$, where N_{eff} is the effective number of the MoS_2 NP layers, we then have $I_{\text{total}} \approx N^2_{\text{eff}} I_{\text{monolayer}}$. The corresponding third-order susceptibility of the MoS_2 NPs can be estimated by $\chi^{(3)}_{\text{total}} = N^2_{\text{eff}} \chi^{(3)}_{\text{monolayer}}$. Therefore, the third-order susceptibility for the NPs formed by monolayer MoS_2 can be calculated with the following equation

$$\chi^{(3)}_{\text{monolayer}} = \frac{n_0^2 n_2 (\text{cm}^{-2}/W^{-1})}{0.0395 \times N^2_{\text{eff}}} \quad (3)$$

The transmittance spectrum of the MoS_2 NP suspension is shown in Fig. 1(d). The effective layer number N_{eff} was quantitatively estimated to be 54–83 at the selected wavelengths ranging from 720–800 nm. As a result, the third-order susceptibility of the MoS_2 NP dispersions was estimated to be in the order of 1×10^{-7} esu, which also reflects a two orders of magnitude enhancement compared with the corresponding popular 2D materials with planar features.[10] For a clear comparison, Fig. 3(b) shows that the nonlinear optical response of the MoS_2 NPs demonstrates a distinct increase with the wavelength redshift. Similar results were obtained when the solvent was replaced by methylbenzene or distilled water. Additionally, the n_2 of ethanol is almost 9 orders of magnitude smaller than the counterpart of the MoS_2 nanosheets, so the contribution of the solvent to the nonlinearity calculation can be reasonably ignored. Table 1 shows the nonlinear refractive index (n_2) and third-order nonlinear susceptibility ($\chi^{(3)}_{\text{monolayer}}$) for different 2D materials measured by the SSPM method. Consequently, a comprehensive comparison justifies that n_2 and $\chi^{(3)}_{\text{monolayer}}$ of the MoS_2 nanostructure with curved features are orders of magnitude larger than the other similar 2D planar featured materials. Convincingly, it is reasonable to expect that endowing curved features to nano-scaled planar TMDs materials can effectively improve their corresponding nonlinear optical response. The superior $\chi^{(3)}_{\text{monolayer}}$ induced by the newly added freedom also provided a fresh perspective and possibility to stimulate more potential nanoscale materials for optoelectronic applications.

Distortion dependent on light intensity

Based on the investigation of the SSPM phenomenon, a dramatic change of nonlinear refractive index caused by the non-axis symmetrical thermal convection and gravity effect had a major contribution to the distortion of the SSPM diffraction rings. By laser heating the MoS_2 NP dispersions, the thermal convection induced by the laser beam was akin to the asymmetry convection model near a suddenly heated horizontal wire.[24] During the convection process, the upward thermal current due to the molecular density made the upper part of the laser beam temperature gradient smoother, while those below the laser beam remained stationary. MoS_2 NPs in the upper part of laser beam were entrapped by the convection flow, and continuously moved downwards to the lower part. The reduced MoS_2 NP density contributed to a decrease in N_{eff} and n_2, and consequently the modulated phase of the optical field in the upper part was degraded. Therefore, the lower part of the dispersion containing more NPs had a relatively stronger nonlinearity to ignite more diffraction rings, which expressed in the experimental phenomenon as the diffraction pattern squeezed from the top towards the center. Since the half-cone angle of the diffraction pattern is only proportional to n_2 and not n_0,[25] n_2 could be tuned by changing the MoS_2 NP concentration caused by the laser-heating convection. We further investigated the impact of this effect on the variation of the nonlinear refractive index of the MoS_2 NPs, as shown in Fig. 4.

Fig. 2(a) presents a schematic of the distortion process. The maximum value of the vertical radius of the outermost ring and its half-cone angle are denoted by R_{H} and $\theta_{\text{H}}\theta_{\text{H}}$, respectively. The half-cone angle of the diffraction rings can also be estimated by the following: $\theta_{\text{H}} = \lambda/2\pi(d\Delta\varphi/\mathrm{d}r)_{\max}$. Considering the Gaussian beam model, it can be compacted as $\theta_{\text{H}} \approx n_2 \text{IC}$, where $C = -\frac{8rL_{\text{eff}}}{\omega_0^2}\exp\left(\frac{2r^2}{\omega_0^2}\right)_{\max}$, with $r \in [0, +\infty)$ being a constant. Thus, the collapse angle can be obtained as $\theta_{\text{D}} \approx \Delta n_2 \text{IC}$, where Δn_2 is the intensity variation-induced nonlinear refractive index change. Lastly, the change proportion of the nonlinear refractive index can be calculated as follows $\Delta n_2/n_2 = \theta_{\text{D}} < \theta_{\text{H}}$.

The variation ratio of $\Delta n_2/n_2$ with increasing incident intensity has been demonstrated to be a positive nonlinear correlation at different wavelengths in Fig. 4. On the other hand, as the

Table 1 Comparison of the reported n_2 and $\chi^{(3)}_{\text{monolayer}}$ for different 2D materials obtained by SSPM

2D material	Laser type	n_2 (cm^{-2} W^{-1})	$\chi^{(3)}_{\text{monolayer}}$ (esu)	Ref.
$Ti_3C_2T_x$ nanoflakes	Pulsed (fs)	$\sim 10^{-18}$	$\sim 10^{-15}$	22
Bi_2Te_3 nanosheets	CW Pulsed (fs)	$\sim 10^{-13}/10^{-15}$	$\sim 10^{-8}/10^{-9}$	23
MoS_2 nanosheets	CW	$\sim 10^{-7}$	$\sim 10^{-9}$	10
WS_2 nanosheets	CW	$\sim 10^{-7}$	$\sim 10^{-9}$	10
WS_2 NPs	Pulsed	$\sim 10^{-5}$	$\sim 10^{-7}$	13
MoS_2 NPs	Pulsed	$\sim 10^{-5}$	10^{-7}	This work

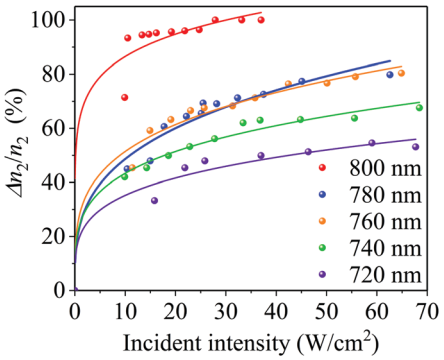

Fig. 4 Dependence of $\Delta n_2/n_2$ on the incident intensity at different wavelengths.

incident laser intensity increased, the change ratio of the nonlinear refractive index first increased and gradually saturated due to the limitation of $\theta_D < \theta_H$. With the redshift of the wavelength, thermal convection became more intense, and the saturation intensity of $\Delta n_2/n_2$ was more likely to be approached.

MoS_2 NP-based all-optical modulation

Applying the strong nonlinear third-order susceptibility of the MoS_2 NPs, an all-optical modulation was experimentally realized based on the SXPM effect. Fig. 5(a) illustrates the all-optical modulator configuration with a single wavelength laser source (λ = 740 nm). The laser beam was equally split into two parts *via* a beam split (BS) (50 : 50). By inserting an optical attenuator, the two beams could be distinguished by their strong and weak power, and were correspondingly defined as the pump and probe light. When the pump and probe lights were simultaneously focused on the sample, the varying intensity of the pump light could affect the nonlinear characteristics of the dispersion, and further manipulate the nonlinear phase change of the probe light, which was explicitly manifested in

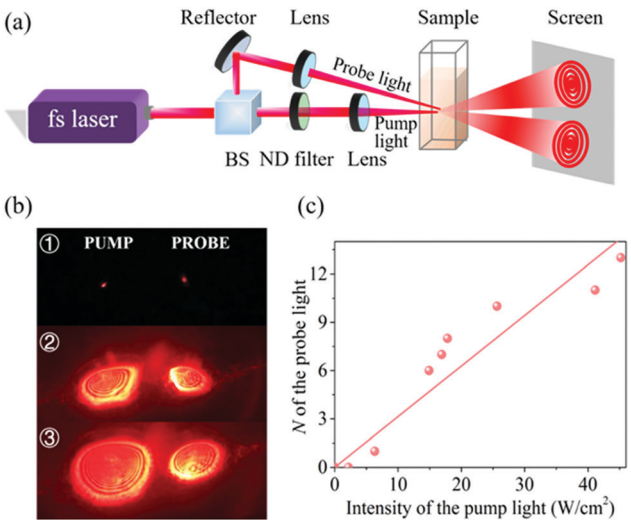

Fig. 5 Single light-based all-optical modulation. (a) Schematic of the experimental setup for SXPM. (b) The transformation process of the diffraction rings. (c) Modulation results between the pump and probe light.

the ring number N. As the intensity of the pump light increased, both the ring number N and the pattern size of the probe light grew. The transformation processes of the two diffraction patterns are displayed in Fig. 5(b). We slowly increased the pump intensity while the probe light intensity was fixed at 5.94 W cm^{-2}. Fig. 5(c) shows the modulation relationship between the pump light and the probe light, suggesting a linear increase. The modulation results imply prospective applications in nonlinear phase change based on the MoS_2 NPs.

The third-order NLO susceptibility can be estimated by $\chi^{(3)} \approx Ne^4/\varepsilon_0 m^3\omega^6 d^2\chi^{(3)} \approx Ne^4/\varepsilon_0 m^3\omega^6 d^2$,[1] where e is the element charge; N stands for the density of electrons of the material at the laser frequency ω; d is the lattice constant; ε_0 is the vacuum permittivity; and m is the effective mass of the conduction electron. Owing to the distortion and curved features in the MoS_2 NPs, the effective mass of the electrons in the 3D featured 2D MoS_2 NPs will reduce in comparison with their planar 2D material counterparts. Based on our previous work on WS_2 NPs,[13] obvious enhancement of the third-order nonlinear susceptibility was also verified due to the introduction of the curved feature compared with the relevant planar 2D WS_2 nanosheets. Comprehensively considering the existing conclusions, we postulate that endowing 3D features to planar 2D TMDs can indeed contribute to the improvement of the third-order NLO properties. Meanwhile, the strong nonlinearity based on the curved-surface effect has been well demonstrated to be applied on SXPM, which is of great significance in exploring light-control-light devices.

The essential mechanism for the SSPM process is generally accepted to be the "wind-chime" model, which proposes collective nonlocal ac electron coherence to account for the macroscopic phase modulation.[11] Each MoS_2 NP acts as a separate domain consisting of charge carriers, such as electrons, holes and electron–hole pairs. These carriers in different or the same domains are totally out of phase, so every single domain has an independent orientation. Once the medium is stimulated by the applied electric field, charged carriers are influenced by the external field and the electron coherence is completely set up within and among each of the different domains. Instead of the original arbitrary orientation between the domains and the field, the domains are reoriented and aligned according to the applied field as if isotropic and coherent.

Conclusions

In conclusion, a novel type of MoS_2 nanostructures with curved features has been synthesized and investigated in detail using the SSPM and SXPM effects. The nonlinear refractive index n_2 and the third-order susceptibility $\chi^{(3)}$ of the MoS_2 NPs have been reliably estimated to be 10^{-5} cm^{-2} W^{-1} and 10^{-7} esu, respectively, which are orders of magnitude larger than those of other planar featured 2D nanomaterials. The relative variation of the effective nonlinear refractive index $\Delta n_2/n_2$ of the MoS_2 NP suspension can be modulated by controlling the intensity of

applied optical fields. Moreover, applying the strong nonlinear response of the MoS_2 NPs, an all-optical modulation based on SXPM further confirms the modulation effect in MoS_2 NP dispersions. Our work provides a pivotal route for future investigations for further improving the NLO response of 2D materials and a necessary support on outstanding application prospects.

Conflicts of interest

There are no conflicts to declare.

Acknowledgements

Fundamental Research Funds for the Central Universities (xzy022021039); Shaanxi Key Science and Technology Innovation Team Project (2021TD-56); Young Talent Recruiting Plans of Xi'an Jiaotong University.

References

1 R. W. Boyd, *Nonlinear Optics*, Academic Press, 2020.
2 T. Li, X. Zhao, Y. Zheng and X. Chen, *Opt. Express*, 2015, **23**, 23827–23833.
3 E. Drobnyh, R. Pachter and M. Sukharev, *J. Phys. Chem. C*, 2019, **123**, 6898–6904.
4 X.-P. Zhai, B. Ma, Q. Wang and H.-L. Zhang, *Phys. Chem. Chem. Phys.*, 2020, **22**, 22140–22156.
5 S. Yamashita, *APL Photonics*, 2019, **4**, 034301.
6 P. Sriram, A. Manikandan, F. C. Chuang and Y. L. Chueh, *Small*, 2020, **16**, 1904271.
7 Q. Liang, Q. Zhang, X. Zhao, M. Liu and A. T. Wee, *ACS Nano*, 2021, **15**, 2165–2181.
8 P. Qi, Y. Luo, B. Shi, W. Li, D. Liu, L. Zheng, Z. Liu, Y. Hou and Z. Fang, *eLight*, 2021, **1**, 1–12.
9 A. Autere, H. Jussila, Y. Dai, Y. Wang, H. Lipsanen and Z. Sun, *Adv. Mater.*, 2018, **30**, 1705963.
10 G. Wang, S. Zhang, X. Zhang, L. Zhang, Y. Cheng, D. Fox, H. Zhang, J. N. Coleman, W. J. Blau and J. Wang, *Photonics Res.*, 2015, **3**, A51–A55.
11 Y. Wu, Q. Wu, F. Sun, C. Cheng, S. Meng and J. Zhao, *Proc. Natl. Acad. Sci. U. S. A.*, 2015, **112**, 11800–11805.
12 J. Song, L. Zhang, Y. Xue, Q. Y.-S. Wu, F. Xia, C. Zhang, Y.-L. Zhong, Y. Zhang, J. Teng and M. Premaratne, *ACS Photonics*, 2016, **3**, 1986–1992.
13 T. Li, R. Hao, L. Zhang, J. Mao, F. Li, Y. Zhang, J. Fang and L. Zhang, *Photonics Res.*, 2020, **8**, 1881–1887.
14 R. Hao, L. Zhang, L. Zhang, H. You, J. Fan and J. Fang, *Nanoscale*, 2020, **12**, 9038–9047.
15 R. Wu, Y. Zhang, S. Yan, F. Bian, W. Wang, X. Bai, X. Lu, J. Zhao and E. Wang, *Nano Lett.*, 2011, **11**, 5159–5164.
16 L. Wu, X. Jiang, J. Zhao, W. Liang, Z. Li, W. Huang, Z. Lin, Y. Wang, F. Zhang and S. Lu, *Laser Phys. Lett.*, 2018, **12**, 1800215.
17 Y. Shi, Y. Wan, R. Liu, B. Tu and D. Zhao, *J. Am. Chem. Soc.*, 2007, **129**, 9522–9531.
18 S. S. Chou, M. De, J. Kim, S. Byun, C. Dykstra, J. Yu, J. Huang and V. P. Dravid, *J. Am. Chem. Soc.*, 2013, **135**, 4584–4587.
19 G. Ma, X. Yan, Y. Li, L. Xiao, Z. Huang, Y. Lu and J. Fan, *J. Am. Chem. Soc.*, 2010, **132**, 9596–9597.
20 C. Lee, H. Yan, L. E. Brus, T. F. Heinz, J. Hone and S. Ryu, *ACS Nano*, 2010, **4**, 2695–2700.
21 S. Durbin, S. Arakelian and Y. Shen, *Opt. Lett.*, 1981, **6**, 411–413.
22 J. Li, Z. Zhang, J. Yi, L. Miao, J. Huang, J. Zhang, Y. He, B. Huang, C. Zhao and Y. Zou, *Nanophotonics*, 2020, **9**, 2415–2424.
23 B. Shi, L. Miao, Q. Wang, J. Du, P. Tang, J. Liu, C. Zhao and S. Wen, *Appl. Phys. Lett.*, 2015, **107**, 151101.
24 C. M. Vest and M. Lawson, *Int. J. Heat Mass Transfer.*, 1972, **15**, 1281–1283.
25 G. Wang, S. Zhang, F. A. Umran, X. Cheng, N. Dong, D. Coghlan, Y. Cheng, L. Zhang, W. J. Blau and J. Wang, *Appl. Phys. Lett.*, 2014, **104**, 141909.